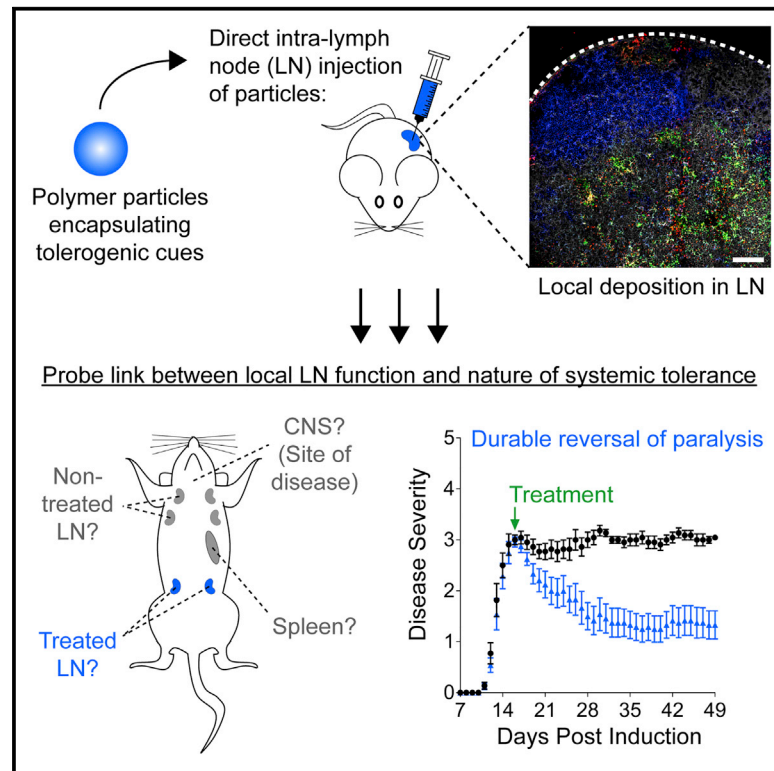# Cell Reports

# Reprogramming the Local Lymph Node Microenvironment Promotes Tolerance that Is Systemic and Antigen Specific

## Graphical Abstract

## Authors

Lisa H. Tostanoski, Yu-Chieh Chiu, Joshua M. Gammon, Thomas Simon, James I. Andorko, Jonathan S. Bromberg, Christopher M. Jewell

## Correspondence

cmjewell@umd.edu

## In Brief

Tostanoski et al. show that a single direct injection of degradable particles into lymph nodes reverses paralysis in a mouse model of multiple sclerosis underpinned by myelin attack. This local reprogramming of the lymph node microenvironment toward regulatory function drives tolerance that is systemic but myelin specific.

## Highlights

- A single intra-lymph node (*i.LN.*) particle dose reverses autoimmunity/paralysis in mice

- Efficacy is dependent on delivery of encapsulated self-antigen to lymph nodes (LNs)

- *i.LN.* delivery of particles reprograms local LN cell composition and function

- Altered local function in LNs promotes systemic but antigen-specific tolerance

CrossMark

**Cell**Press

# Reprogramming the Local Lymph Node Microenvironment Promotes Tolerance that Is Systemic and Antigen Specific

Lisa H. Tostanoski,[1] Yu-Chieh Chiu,[1] Joshua M. Gammon,[1] Thomas Simon,[2,3] James I. Andorko,[1] Jonathan S. Bromberg,[2,3,4,5] and Christopher M. Jewell[1,4,5,6,7,*]

[1]Fischell Department of Bioengineering, University of Maryland, 8228 Paint Branch Drive, College Park, MD 20742, USA
[2]Department of Surgery, University of Maryland School of Medicine, 29 South Greene Street, Baltimore, MD 21201, USA
[3]Center for Vascular and Inflammatory Diseases, University of Maryland School of Medicine, 800 West Baltimore Street, Baltimore, MD 21201, USA
[4]Department of Microbiology and Immunology, University of Maryland School of Medicine, 685 West Baltimore Street, Baltimore, MD 21201, USA
[5]Marlene and Stewart Greenebaum Cancer Center, 22 South Greene Street, Baltimore, MD 21201, USA
[6]United States Department of Veteran Affairs, 10 North Greene Street, Baltimore, MD 21201, USA
[7]Lead Contact
*Correspondence: cmjewell@umd.edu
http://dx.doi.org/10.1016/j.celrep.2016.08.033

## SUMMARY

Many experimental therapies for autoimmune diseases, such as multiple sclerosis (MS), aim to bias T cells toward tolerogenic phenotypes without broad suppression. However, the link between local signal integration in lymph nodes (LNs) and the specificity of systemic tolerance is not well understood. We used intra-LN injection of polymer particles to study tolerance as a function of signals in the LN microenvironment. In a mouse MS model, intra-LN introduction of encapsulated myelin self-antigen and a regulatory signal (rapamycin) permanently reversed paralysis after one treatment during peak disease. Therapeutic effects were myelin specific, required antigen encapsulation, and were less potent without rapamycin. This efficacy was accompanied by local LN reorganization, reduced inflammation, systemic expansion of regulatory T cells, and reduced T cell infiltration to the CNS. Our findings suggest that local control over signaling in distinct LNs can promote cell types and functions that drive tolerance that is systemic but antigen specific.

## INTRODUCTION

Multiple sclerosis (MS) is an autoimmune disease that occurs when self-reactive CD4^{+} T cells enter the CNS, recognize myelin self-antigen, secrete inflammatory cytokines, and recruit additional infiltrating myelin-specific T cells and antibodies (Comabella and Khoury, 2012; Dendrou et al., 2015). These effects drive demyelination of neurons, destruction of oligodendrocytes, and loss of motor function that traditionally have been treated using non-specific, systemic immunosuppression (Piehl, 2014). The need for more effective and selective therapeutic options has

sparked intense interest in vaccine-like strategies that promote myelin-specific tolerance (Lutterotti and Martin, 2014; Steinman et al., 2012). For example, several recent reports have studied the administration of myelin, cytokines, or immunomodulatory drugs to bias T cell differentiation away from inflammatory subsets (e.g., $T_H1$ and $T_H17$) and toward regulatory T cells ($T_{REGS}$) without broad suppression (Esposito et al., 2010; Ho et al., 2005; Lutterotti and Martin, 2014; Northrup et al., 2016).

Recently, nanoparticles (NPs) have been explored as carriers of self-antigens or tolerogenic signals (Gammon et al., 2015; Getts et al., 2012; Hunter et al., 2014; Kontos et al., 2013; Look et al., 2013; Maldonado et al., 2015; Northrup et al., 2014; Tsai et al., 2010; Yeste et al., 2012) because biomaterials can enhance delivery and targeting of cell types (e.g., dendritic cells [DCs]) that play an important role in controlling tolerance (Andorko et al., 2015; Manicassamy and Pulendran, 2011; Northrup et al., 2016). Findings from several studies indicate NP-mediated co-delivery of self-antigen and regulatory cues drives a synergistic effect in restraining mouse models of MS (Maldonado et al., 2015; Yeste et al., 2012). However, other reports, such as those of Miller, Shea, and colleagues, demonstrate that NPs loaded with or displaying self-antigen alone can promote tolerance (Clemente-Casares et al., 2016; Getts et al., 2012; Hunter et al., 2014). Thus, the unique role of each component in controlling self-reactivity is unclear. Whereas these past approaches used systemic or peripheral injection routes, here we used direct lymph node (LN) delivery as a tool to isolate the impact of self-antigen and regulatory cues on the local function of injected LNs, the resultant effects on non-treated tissues, and, ultimately, the progression of disease.

This approach was motivated by the fact that T cell polarization occurs in the spleen and LNs, tissues that coordinate adaptive immunity (Mueller and Germain, 2009) but that are anatomically distinct from the site of attack in MS and other tissue-specific autoimmune diseases. Thus, LNs play a critical role in defining the inflammatory or regulatory functions of T cells that eventually migrate to sites of disease. This relationship is further evidenced by the clinical success of natalizumab, a monoclonal antibody
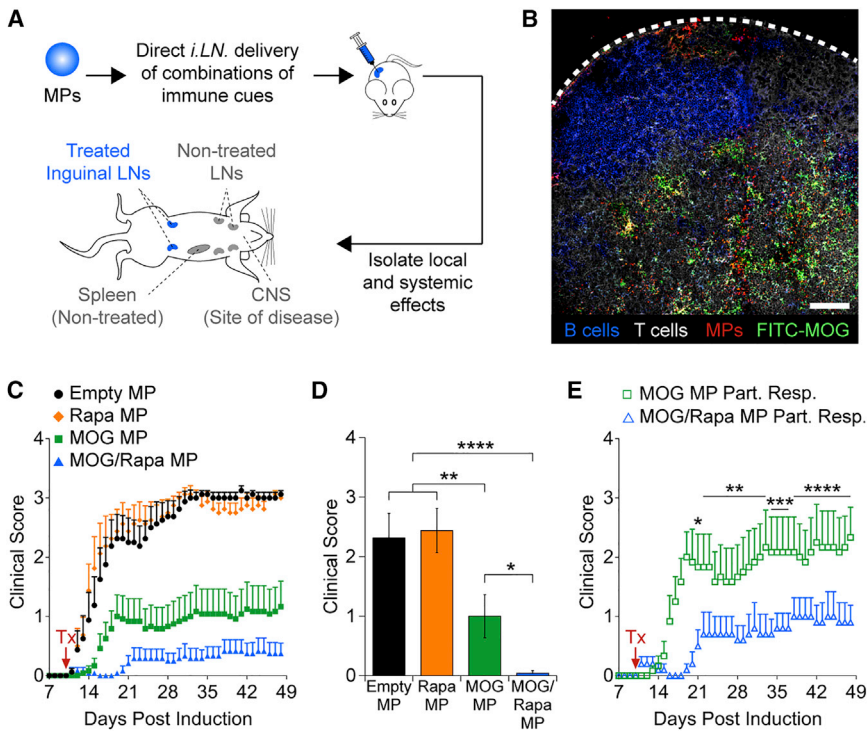
**Figure 1. Intra-nodal Injection of MPs to Promote Tolerance**

(A) Direct control over LN signaling via *i.LN.* injection of MPs encapsulating immune cues is shown.

(B) Immunofluorescent image shows inguinal LN excised 30 min after *i.LN.* injection with fluorescent MPs (red) encapsulating fluorescent MOG peptide (green) and Rapa. B cells, B220 (blue); T cells, CD3e (white). Scale bar, 100 μm.

(C) Mean clinical score of mice induced with EAE and treated *i.LN.* on day 10 (Tx, red arrow) with empty MPs (n = 8), MOG MPs (n = 12), Rapa MPs (n = 8), or MOG/Rapa MPs (n = 12). Statistics are shown in (D) and (E) for clarity.

(D) Mean clinical scores at day 19 are shown.

(E) Mean clinical scores of mice in (C) that developed symptoms (Part. Resp.) after MOG MP or MOG/Rapa MP treatment.

Statistical analysis in (D) was performed using one-way ANOVA with a Tukey post-test and in (E) using multiple t tests, one at each time point, with a Holm-Sidak post-test correction for multiple comparisons. Data in all panels represent mean ± SEM (*$p \leq 0.05$, **$p \leq 0.01$, ***$p \leq 0.001$, and ****$p \leq 0.0001$). See also Table S1 and Figures S1 and S2.

that non-specifically blocks lymphocyte migration across the blood-brain barrier (Cross and Naismith, 2014), underscoring the link between pathogenic cells armed in the periphery and infiltration into the CNS to drive disease. In addition, a network of lymphatic vessels recently was discovered in the brains of mice and shown to communicate directly with peripheral LNs (Aspelund et al., 2015; Louveau et al., 2015). This landmark finding suggests new routes by which myelin self-antigen might exit the CNS for processing in draining LNs, where the local microenvironment controls the response to incoming antigens. However, direct study of the link between local LN signaling and systemic tolerance previously has been hindered by poor control over how therapeutic cues are trafficked to and processed in LNs following injection via conventional routes.

We recently reported that direct, intra-LN (*i.LN.*) delivery of degradable polymer depots can be used to retain encapsulated adjuvants in LNs and drive potent expansion of antigen-specific effector T cells against model antigens (Andorko et al., 2014; Jewell et al., 2011). We hypothesized this platform could be exploited to study how spatially localized self-antigen and tolerogenic immune cues in LNs impact the progression of autoimmune disease. Since many vaccines and immunotherapies must ultimately reach LNs or spleen for efficacy, this knowledge could inform new therapies, irrespective of injection route, while also indicating the clinical potential of controlling local LN function with polymer depots. Using two immune cues widely studied in recent tolerogenic vaccines, a peptide fragment of myelin oligodendrocyte glycoprotein (MOG) and rapamycin (Rapa), we show that a single *i.LN.* dose of particles administered at the peak of disease reverses disease-induced paralysis. In our research, efficacy is dependent on localization of depots

to LNs, requires encapsulation of myelin self-antigen, and is enhanced when Rapa is co-incorporated in depots along with MOG. Underlying the functional effects is a local reorganization in cell composition of the injected LNs that results in systemic restraint of inflammation and polarization of CD4$^+$ T cells toward T$_{REGS}$. These changes also are accompanied by the formation of tolerogenic structural subdomains in both treated LNs and non-treated CNS-draining LNs, as well as a decrease in the frequency of T cells infiltrating CNS tissue.

## RESULTS

### *i.LN.* Injection of Depots Co-loaded with MOG and Rapa Confers Synergistic Restraint of Autoimmunity

Our previous studies using inflammatory signals for pro-immune vaccination revealed that particles with diameters of several microns or more maximized retention in LNs following *i.LN.* injection (Jewell et al., 2011). Thus, a double-emulsion process was used to prepare degradable poly(lactide-co-glycolide) microparticle (MP) depots in this size range, encapsulating various combinations of MOG and Rapa. MP formulations were then introduced into the inguinal LNs of mice (Andorko et al., 2014; Jewell et al., 2011), utilizing a common model of MS, experimental autoimmune encephalomyelitis (EAE). We used this approach to study the local impact of each component on treated nodes, corresponding changes in non-injected LNs, spleen, and CNS, as well as how these effects alter the nature and specificity of systemic tolerance during CNS autoimmunity (Figure 1A).

Immunofluorescent analysis was first used to confirm *i.LN.* injection localized MPs in LNs. Fluorescently labeled MPs and cargo were detected dispersed throughout the LN paracortex,

without disrupting the classic arrangement of B and T cell zones (Figure 1B). Myelin self-antigen and Rapa are two of the most intensely studied molecules in tolerance therapies, having been explored independently in models of MS and also recently shown to exert synergistic effects when administered systemically (Maldonado et al., 2015). Thus, we next designed experiments to decipher the roles of MOG and Rapa in the development and maintenance of tolerance following *i.LN.* injection. Mice were induced with EAE and 10 days later, to mimic an early therapeutic intervention, immunized *i.LN.* with MPs encapsulating MOG, Rapa, or both (Table S1). A control group of empty MPs (i.e., polymer and stabilizer only) exhibited no significant effect on the severity of clinical scores compared with induced, untreated mice (Figure S1). Similarly, MPs encapsulating Rapa alone had no impact on EAE measured by clinical score (Figures 1C and 1D), incidence of disease (Figure S2), and weight loss—an indirect indicator of disease (Figure S2).

In contrast, both MOG MPs and MOG/Rapa MPs markedly and permanently reduced the onset and severity of clinical EAE scores (Figures 1C and S2) and weight loss (Figure S2), with co-loaded MPs conferring a synergistic therapeutic effect in attenuating disease severity. In particular, at time points corresponding to the development of EAE symptoms in MOG MP-treated mice, MOG/Rapa MP-treated mice remained almost completely asymptomatic (Figures 1D and S2). Although MOG/Rapa MPs generally delayed disease onset relative to MOG MPs, there was only a modest difference in the final incidence of disease between the two groups, 33.3% versus 50%, respectively (Figure S2). The MOG/Rapa MP treatment exhibited a trend of less severe disease, with a 2.70-point reduction in final mean score relative to empty MP-treated mice, compared with a 1.90-point reduction in MOG MP-treated mice. However, most pronounced was the result that, among mice that did develop disease, termed partial responders, MOG/Rapa MPs (final clinical score of $0.90 \pm 0.29$) significantly decreased the severity of paralysis compared with MOG MPs (final clinical score of $2.33 \pm 0.51$; Figure 1E).

To assess the functional impact of *i.LN.* treatments on pathogenic cell infiltration into the CNS, spinal cords were collected 5 days after MP treatment (i.e., day 15 post-EAE induction), and sections were analyzed for the frequency of T cells. As expected, we observed a significant infiltration of $CD3^+$ cells in empty MP-treated mice (Figures 2A and 2B). Consistent with clinical score data, Rapa MPs did not reduce $CD3^+$ cell infiltration, resulting in frequencies that were similar to that of sections from empty MP-treated mice. Both MOG MPs and MOG/Rapa MPs drove a significant reduction in infiltration compared with empty MP- and Rapa MP-treated mice (Figure 2B). Compared with MOG MPs, a trend of reduced infiltration was observed when co-loaded MPs were administered, though this result was not statistically significant. Thus, *i.LN.* delivery of MPs drove significant changes in the pathogenic T cell populations at a site that is anatomically distinct from the injection site, inguinal LNs, which are non-CNS-draining nodes.

### Localization of Self-Antigen and Rapa in LNs Alters Tissue Composition

The decrease in T cells in the CNS motivated study of how the frequency and number of T cells changed in LNs, a key site of T cell expansion and polarization. To analyze the impact of these signals on the cellular composition of injected LNs, mice were treated on day 10, then flow cytometry was used to measure the frequency and number of T cell and antigen-presenting cell (APC) populations in the treated LN (Figure 2C). MOG MPs, Rapa MPs, and MOG/Rapa MPs all drove a local decrease in the frequency of $CD4^+$ T cells compared with empty MP controls (Figures 2D and S3); this decrease was greatest in mice treated with MOG/Rapa MPs. MOG/Rapa MPs were also the only formulation that caused a significant decrease in the frequency of $CD8^+$ T cells in treated LNs (Figures 2E and S3). Despite the reduced frequencies in both T cell subsets, we observed a statistically similar number of cells in MOG/Rapa MP-treated LNs relative to empty MPs and an increase in the number of $CD4^+$ (Figure 2F) and $CD8^+$ (Figure 2G) T cells following MOG MP treatment. This reduction in frequency, but similar or increased number of T cells, led us to hypothesize that another immune cell type (i.e., APCs) was increasing in both frequency and number to account for some or all of the remaining cell population.

Relative to treatment of LNs with empty MPs, both MOG MPs and MOG/Rapa MPs significantly increased the frequency of cells expressing a classic DC marker (CD11c) (Figure 2H); Rapa MPs also increased the frequency of DCs, but not to a level that was statistically significant (Figure 2H). Similar outcomes were observed in analyzing the number of $CD11c^+$ cells (Figure 2J), as well as the number and frequency of cells expressing a classic macrophage marker (F4/80), but only MOG MPs caused a significant increase in these populations (Figures 2I and 2K). These results were generally consistent with the idea that T cell frequencies, but not numbers, decreased in treated nodes, while APC populations increased. Taken together, our findings in Figures 1 and 2 confirm a critical role for self-antigen in controlling EAE, including reorganization of cellular composition in injected LNs and infiltration of T cells into the CNS, as well as a synergistic effect conferred by the inclusion of Rapa in depots. These results also suggest that therapeutic efficacy is antigen specific and impacts both innate and adaptive responses. Thus, we selected the most potent formulation, MOG/Rapa MPs, to probe the local tissue- and cell-level changes in LNs that lead to systemic tolerance.

### Localization of Self-Antigen and Rapa in LNs Alters Tissue Organization and Phenotype

To explore the local changes in the organization of treated LNs, mice were injected on day 10, and then histological analysis was carried out on day 15 (Figure 3A). These experiments revealed a classic follicular organization of B cells and T cells with interspersed DCs in LNs treated with empty MPs (Figure 3B). In contrast, LNs injected with MOG/Rapa MPs exhibited increases in DCs (Figure 3C, red signal), consistent with flow cytometry results (Figure 2H). This finding motivated more quantitative study of LN structural organization following MP treatment. Thus, we prepared sections from replicate animal groups, and we analyzed the expression of CD11c, stromal features of LNs, and a prototypical $T_{REG}$ marker, forkhead box P3 (Foxp3) (Figure 3D), among at least 20 sections as a function of area. Similar to preliminary tissue staining (Figures 3B and 3C) and flow cytometry (Figure 2H) results, calculation of the frequency of $CD11c^+$ area revealed a
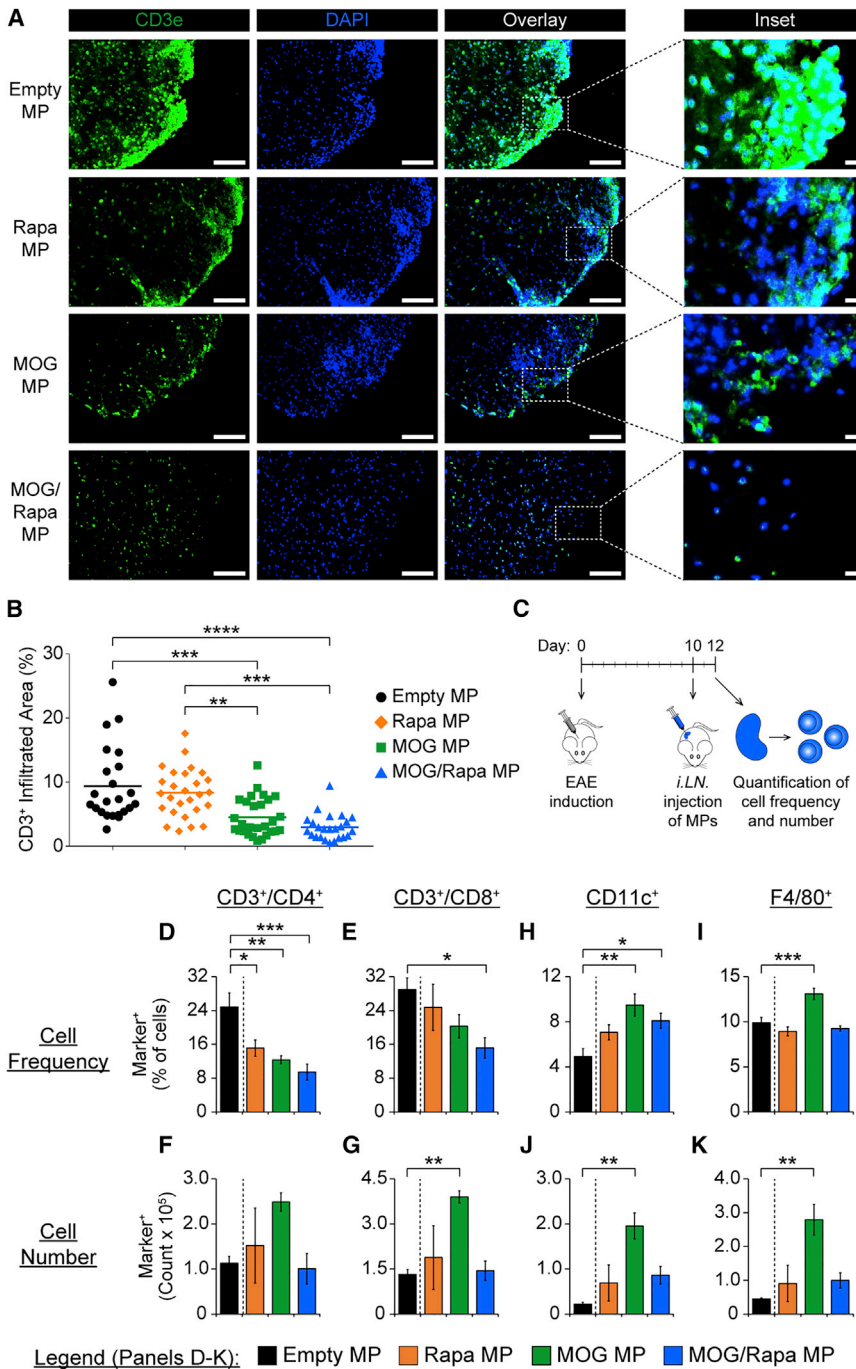
**Figure 2. The *i.LN.* Injection of MPs Restrains Inflammatory Cell Infiltration into the CNS and Alters Local Cell Compartments**

Mice were induced with EAE, treated *i.LN.* with the indicated MP formulations (n = 4) on day 10, and then spinal cords were isolated on day 15.

(A) Immunofluorescent analysis of sections of the spinal cord shows the expression of CD3 (green), DAPI (blue), and an overlay. Scale bar, 100 μm. An inset of the overlay channel is shown on the far right column. Scale bar, 10 μm.

(B) Quantification of the frequency of CD3$^+$ cells in spinal cord sections shown in (A) following treatment with empty MPs (n = 23), MOG MPs (n = 28), Rapa MPs (n = 27), or MOG/Rapa MPs (n = 24). Statistical analysis was performed using one-way ANOVA with a Tukey post-test to compare the means of all groups.

(C) In similar experiments, mice were induced with EAE, treated *i.LN.* with the indicated MP formulations (n = 4–6) on day 10, and then treated LNs were isolated 2 days later.

(D–G) The frequencies of (D) CD4$^+$ T cells (CD3$^+$/CD4$^+$) and (E) CD8$^+$ T cells (CD3$^+$/CD8$^+$) and the numbers of (F) CD4$^+$ and (G) CD8$^+$ T cells were quantified.

(H–K) The frequencies of (H) macrophages (F4/80$^+$) and (I) dendritic cells (DCs, CD11c$^+$) and (J and K) the numbers of these populations in treated LNs were determined. Statistical analyses in (D)–(K) were performed using one-way ANOVA with a Tukey post-test to compare each group to empty MP-treated controls. Data in (D)–(K) represent mean ± SEM (*p ≤ 0.05, **p ≤ 0.01, ***p ≤ 0.001, and ****p ≤ 0.0001).

See also Figure S3.

empty MPs, MOG/Rapa MPs drove a significant increase in the accumulation of Foxp3$^+$ cells in the cortical ridge (Figure 3F).

## Control of Autoimmunity Is Dependent on *i.LN.* Delivery and Encapsulation of Self-Antigen

Our flow cytometry and immunofluorescent analyses led us to hypothesize that local delivery of MOG and Rapa drives recruitment of DCs due to the presence of MOG in animals with active EAE. In addition, the altered cellular composition of treated LNs and increase in the presence of T$_{REGS}$ localized in tolerogenic subdomains motivated analysis of how cells in these tissues respond to an encounter of self-antigen. Thus, we next characterized the inflammatory recall responses in cells isolated from treated LNs at different time points before and after MP treatment. On day 9 (i.e., prior to MP treatment), restimulation of cells from LNs with MOG peptide induced high levels of IL-17 (Figure 4A), GM-CSF (Figure 4B), and IFN-γ (Figure 4C) secretion. In contrast, no effect was observed in response to an irrelevant peptide from ovalbumin

statistically significant increase following MOG/Rapa MP treatment relative to empty MPs (Figure 3E).

To assess whether these local changes in APCs were accompanied by altered expression or localization of T$_{REGS}$, we analyzed the number of Foxp3$^+$ cells per area in the cortical ridge of LNs (Figure 3D)—indicated by co-localization with a stromal marker, ER-TR7—a structural microdomain associated with T$_{REG}$ localization during tolerance (Warren et al., 2014). Enumeration of Foxp3 staining revealed that, relative to treatment with
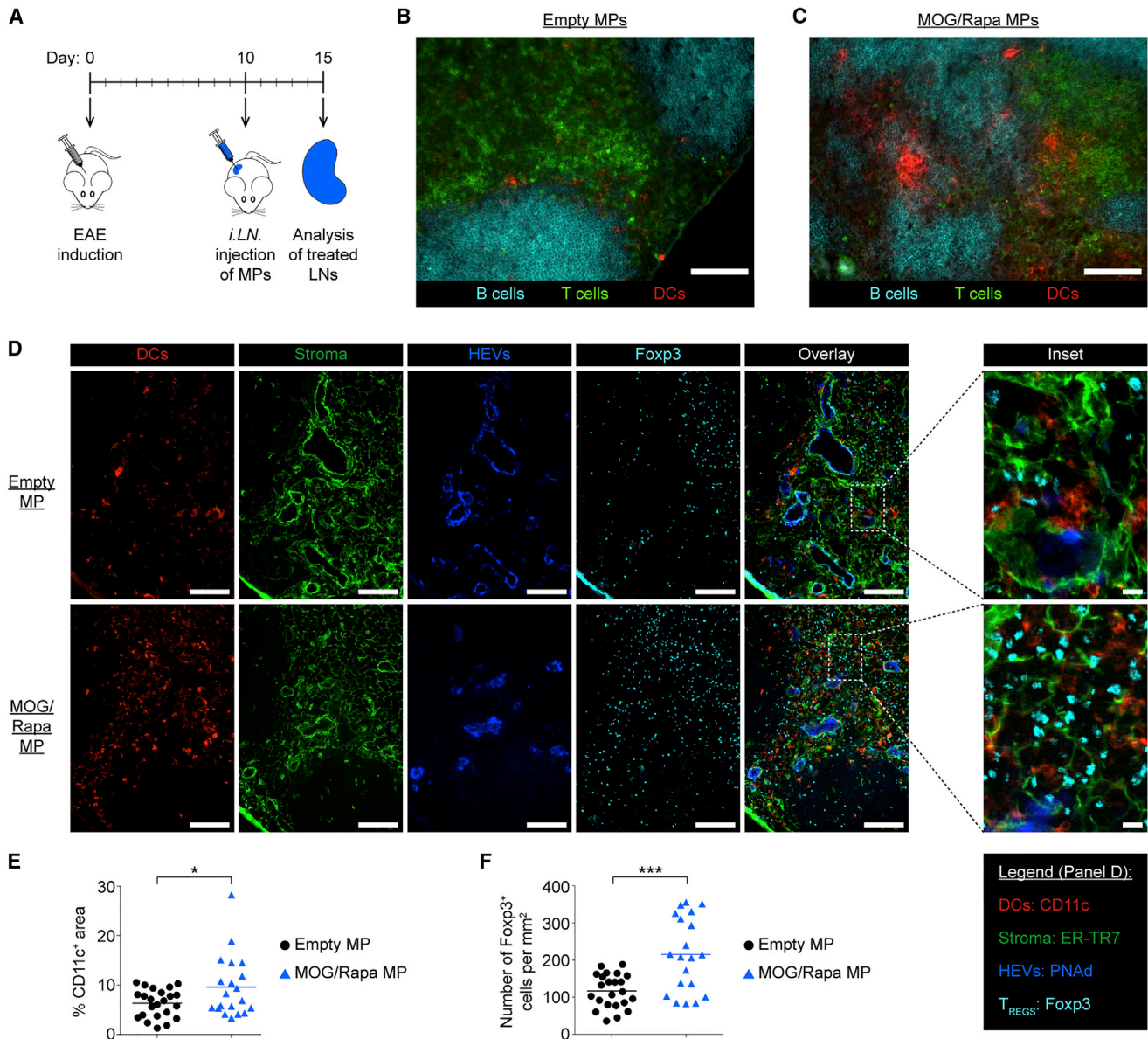
**Figure 3. MOG/Rapa MPs Elicit Changes in the Organization and Composition of Treated LNs**

(A) Mice were treated *i.LN.* on day 10 post-EAE induction, and the injected inguinal LNs were excised on day 15.

(B and C) Immunofluorescent analysis of LNs injected with (B) empty MPs or (C) MOG/Rapa MPs shows B cells (B220$^+$, cyan), T cells (CD3e$^+$, green), and DCs (CD11c$^+$, red). Scale bars, 100 μm.

(D) Images of the cortical ridge of LNs, injected with empty MPs or MOG/Rapa MPs, show DCs (CD11c$^+$, red), reticular fibroblasts (stroma, ER-TR7$^+$, green), high endothelial venules (HEVs, PNAd$^+$, blue), Foxp3$^+$ cells (cyan), and an overlay. Scale bars, 100 μm. An inset of the overlay channel is shown on the far right column. Scale bar, 10 μm.

(E and F) Quantitative image analysis was used determine the frequencies of (E) DCs and (F) Foxp3$^+$ cells following empty MP (n = 23) or MOG/Rapa MP (n = 20) treatment in the cortical ridge of sections like the representative images shown in (D). Statistical analyses in (E) and (F) were two-tailed Student's t tests.

(OVA, Figure S4), consistent with the myelin-specific inflammatory response associated with disease. This local inflammatory response in the inguinal LN is expected in induced MS models, since inguinal LNs drain the peripheral sites used to induce disease. At time points after *i.LN.* injection, MOG/Rapa MPs generally reduced inflammatory cytokine secretion during restimulation relative to treatment with empty MPs (Figures 4A–4C). However, these decreases were significant only on day 15 for IL-17 and GM-CSF. Interestingly, when we analyzed similar cultures prepared from splenocytes, significant reductions in IL-17 were observed at days 12 and 15 (Figure 4D), as well in GM-CSF (Figure 4E) and IFN-γ (Figure 4F) at day 12. Together, these
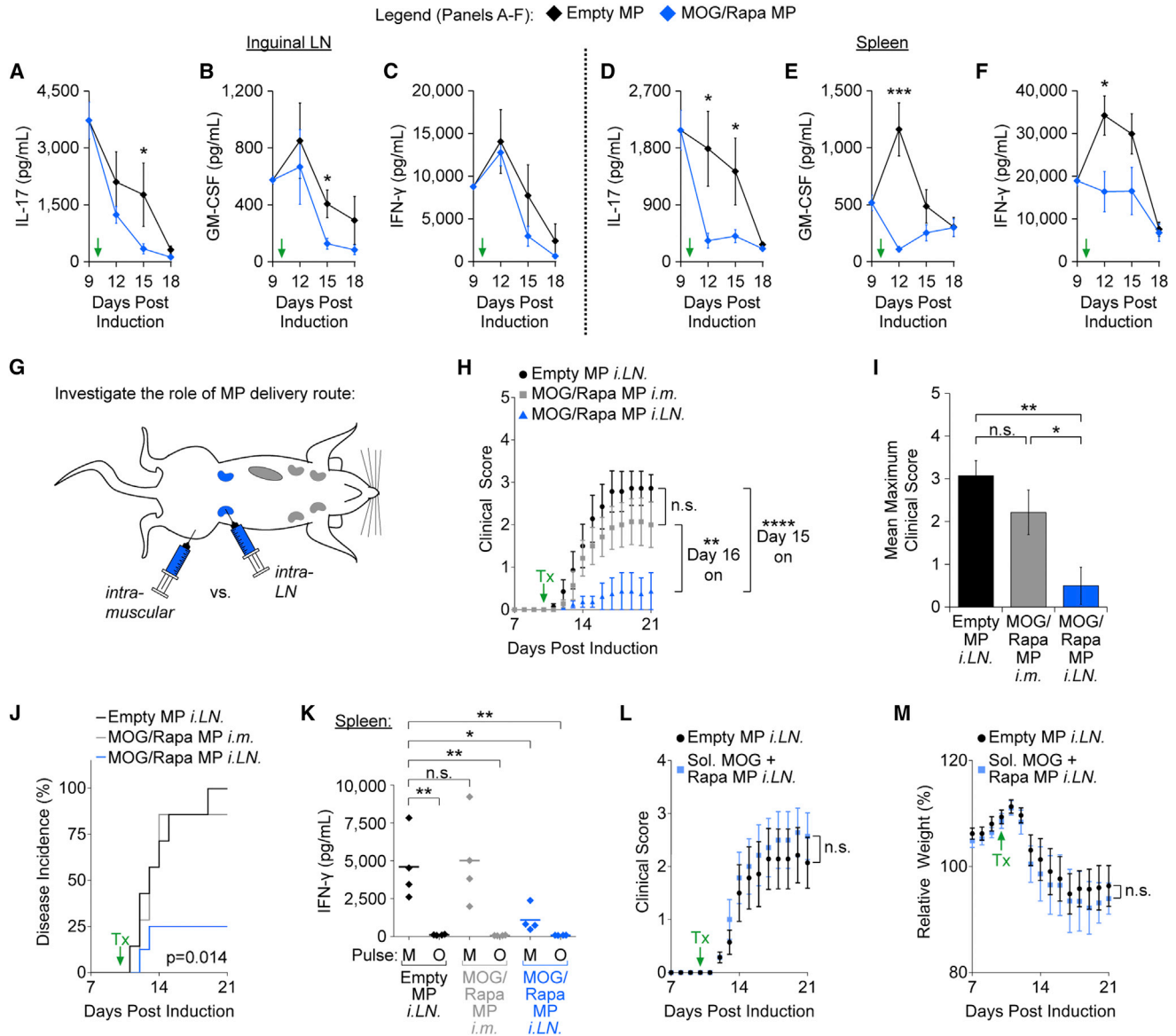
**Figure 4. *i.LN.* Delivery and Antigen Encapsulation Restrain EAE and MOG-Triggered Inflammation**

(A–F) Secretion of (A) IL-17, (B) GM-CSF, and (C) IFN-γ in cells from treated LNs and (D–F) spleens stimulated ex vivo with MOG. Identical groups (n = 3–6) were prepared for each time point and tissues were isolated before (day 9) or after (days 12, 15, and 18) *i.LN.* treatment on day 10. In (A)–(F), t tests were used to compare empty MP and MOG/Rapa MP treatments at each time point.

(G) Benchmarking *i.LN.* injection against peripheral intramuscular (i.m.) injection is shown.

(H–J) The (H) mean clinical score, (I) mean maximum score, and (J) incidence of disease in mice treated on day 10 (Tx, green arrow) post-EAE induction with empty MPs *i.LN.* (n = 7), MOG/Rapa MPs *i.LN.* (n = 8), or an equivalent dose of i.m. MOG/Rapa MPs (n = 7). Statistical analysis in (H) was performed using two-way ANOVA with a Tukey post-test, in (I) with a one-way ANOVA with a Tukey post-test, and in (J) with a log-rank test.

(K) Secretion of IFN-γ after MOG or OVA restimulation of splenocytes on day 21. Statistical analysis in (K) was performed using one-way ANOVA with a Tukey post-test to compare each group to a control group of cells isolated from mice treated with empty MPs *i.LN.* and pulsed with MOG.

(L and M) The (L) mean clinical score and (M) relative body weight of mice induced with EAE and treated *i.LN.* on day 10 with either empty MPs (n = 7) or soluble MOG peptide mixed with Rapa MPs (n = 7). Statistical analyses in (L) and (M) were performed using multiple t tests, one at each time point, with a Holm-Sidak post-test correction for multiple comparisons. Data in all panels represent mean ± SEM (*p ≤ 0.05 and **p ≤ 0.01).

See also Figure S4.

results indicate that local introduction of MOG/Rapa MPs to LNs can control disease while reducing self-antigen-triggered inflammation in both treated and non-treated tissues.

As LN delivery of MPs drove both local and systemic effects, we sought to test the importance of localization of signals in LNs for the development of tolerance. Mice were induced with

EAE and treated on day 10 with MOG/Rapa MPs either *i.LN.* or intramuscularly (i.m.) to mimic a common peripheral vaccination route (Figure 4G). Compared with empty particles administered *i.LN.* i.m. injection of MOG/Rapa MPs provided no significant improvement to disease progression scores (Figure 4H), severity (Figure 4I), or incidence (Figure 4J). In contrast, a matched dose of MOG/Rapa MPs administered *i.LN.* again caused a potent therapeutic impact (Figures 4H–4J). Further, to test how the site of injection impacted systemic protection against inflammation, cells were collected from the spleens on day 21 and restimulated with either MOG or OVA peptide. In cells isolated from mice treated with empty MPs, restimulation with MOG drove a significant increase in the secretion of IFN-γ (Figure 4K) compared with OVA stimulation. The *i.LN.* treatment with MOG/Rapa MPs, but not with i.m. injection, resulted in a significant reduction in IFN-γ secretion following MOG pulse (Figure 4K).

Since attenuation of EAE and inflammatory responses required local *i.LN.* delivery, we next tested whether encapsulation of signals was required for efficacy. Owing to the poor solubility of Rapa and the miniscule volumes used for *i.LN.* injection, we were unable to formulate admixed (i.e., without MPs) treatments of soluble MOG and Rapa as controls. Thus, Rapa MPs were mixed with soluble MOG and administered *i.LN.* 10 days after EAE induction to assess the role of antigen co-encapsulation. We observed no significant differences between empty MP controls and soluble MOG + Rapa MPs with respect to either clinical score (Figure 4L) or relative body weight (Figure 4M). These findings indicate that both antigen encapsulation and local LN injection of MOG/Rapa depots play critical roles in tolerance.

### Restraint of Autoimmunity Is Myelin Specific
Together, our results suggest a scenario where *i.LN.* treatment results in antigen presentation with limited inflammation. We hypothesized that this local LN reprogramming also might drive T$_{REG}$ expansion and the development of tolerance in a myelin-dependent manner. To investigate this hypothesis, we directly studied the importance of including disease-relevant myelin antigen in the restraint of EAE-induced paralysis and underlying changes in immune cell function. Mice were treated on day 10 with empty MPs, MOG/Rapa MPs, or MPs encapsulating Rapa and an irrelevant antigen, OVA (OVA/Rapa MPs). Cells from the treated LNs and spleen were isolated, restimulated with MOG peptide, and then the secretion of inflammatory cytokines was analyzed. Surprisingly, both MOG/Rapa MPs and OVA/Rapa MPs caused significant and equivalent local suppression of IFN-γ (Figure 5A), GM-CSF (Figure 5B), and IL-17 (Figure 5C) compared with empty MP-treated controls. Similar effects were observed in the spleen (Figures 5D–5F), but the differences were more modest, with statistically significant effects only observed for IL-17 (Figure 5F). We also observed a trend that the lowest inflammatory cytokine levels were associated with MOG/Rapa MPs.

Since the inclusion of disease-relevant antigen in depots was not critical to reduce inflammatory recall response, we hypothesized MOG/Rapa depots might more effectively expand T$_{REGS}$ that can control pathogenic populations. This hypothesis was supported by our observation above of significant reorganization of treated LNs with respect to Foxp3 localization in the

cortical ridge following MOG/Rapa MP treatment (Figures 3D and 3F). However, when we analyzed the frequency of CD4$^+$/CD25$^+$Foxp3$^+$ among all cells, rather than in structural microdomains, we observed only a trend of increased T$_{REG}$ frequency after treatment with either MOG/Rapa or OVA/Rapa MPs, findings that were not statistically significant (Figures 5G, 5H, top, and S5). In stark contrast, however, MOG/Rapa MPs significantly increased the frequency of T$_{REGS}$ in non-injected tissues, pooled untreated LNs and spleen, compared with OVA/Rapa MPs and empty MPs (Figures 5G, 5H, middle and bottom, and S5).

We next tested if these changes in immune cell function and phenotype might have differential implications for disease progression. Mice were again induced with EAE, treated with MPs as above, and monitored for disease symptoms. Strikingly, mice treated with empty MPs or OVA/Rapa MPs developed paralysis that was severe and equivalent (Figures 5I–5K), while MOG/Rapa MPs dramatically improved clinical scores (Figure 5I), body weight (Figure 5J), and disease incidence, (Figure 5K).

### *i.LN.* Injection of MOG/Rapa MPs Drives the Accumulation of T$_{REGS}$ in CNS-Draining LNs and Reverses Autoimmunity
Together, the results in Figure 5 support a mechanism by which non-specific suppression occurs at the site of injection due to local Rapa introduction but whereby treatment with MPs also incorporating myelin drives the expansion of T$_{REGS}$ that circulate systemically to other tissues and sites of disease. This hypothesis motivated the study of the frequency and localization of Foxp3 expression in a key non-treated disease-relevant tissue, cervical LNs, which drain the CNS. For these studies, mice were induced with EAE and treated with empty MPs or MOG/Rapa MPs on day 10; 5 days later, the cervical LNs were excised and analyzed by immunofluorescent analysis (Figure 6A). Quantitative analysis of at least 20 sections for each MP treatment revealed a statistically similar frequency of DCs in both MP treatments (Figure 6B) but a large increase in the number of Foxp3$^+$ cells in the cortical ridge of LNs (Figure 6C). These data support the hypothesis that MOG/Rapa depots delivered to non-CNS-draining LNs increase T$_{REG}$ frequencies in distant LNs that drain the sites of disease during MS.

Since local reprogramming of LNs resulted in strong systemic effects that generated antigen-specific control of disease, we last tested if this approach could reverse established disease. In these studies, mice were treated with a single injection of MOG/Rapa MPs or empty MPs at the peak of EAE (day 16). MOG/Rapa MPs drove a dramatic reduction in mean clinical score (Figure 7A), reversing paralysis and promoting weight gain (Figure 7B). Strikingly, while 100% of mice treated with empty MPs exhibited sustained severe disease, 75% of MOG/Rapa MP-treated mice experienced durable reductions in clinical score of at least two points (Figures 7C and 7D). Thus, a single *i.LN.* treatment with MOG/Rapa MPs restored CNS function, even when administered at the peak of disease. Together, these findings suggest that *i.LN.* injection is not only a tool to study the role of specific therapeutic components in tolerance but also a powerful approach to generate antigen-specific control of disease, even when intervention occurs late in established disease.
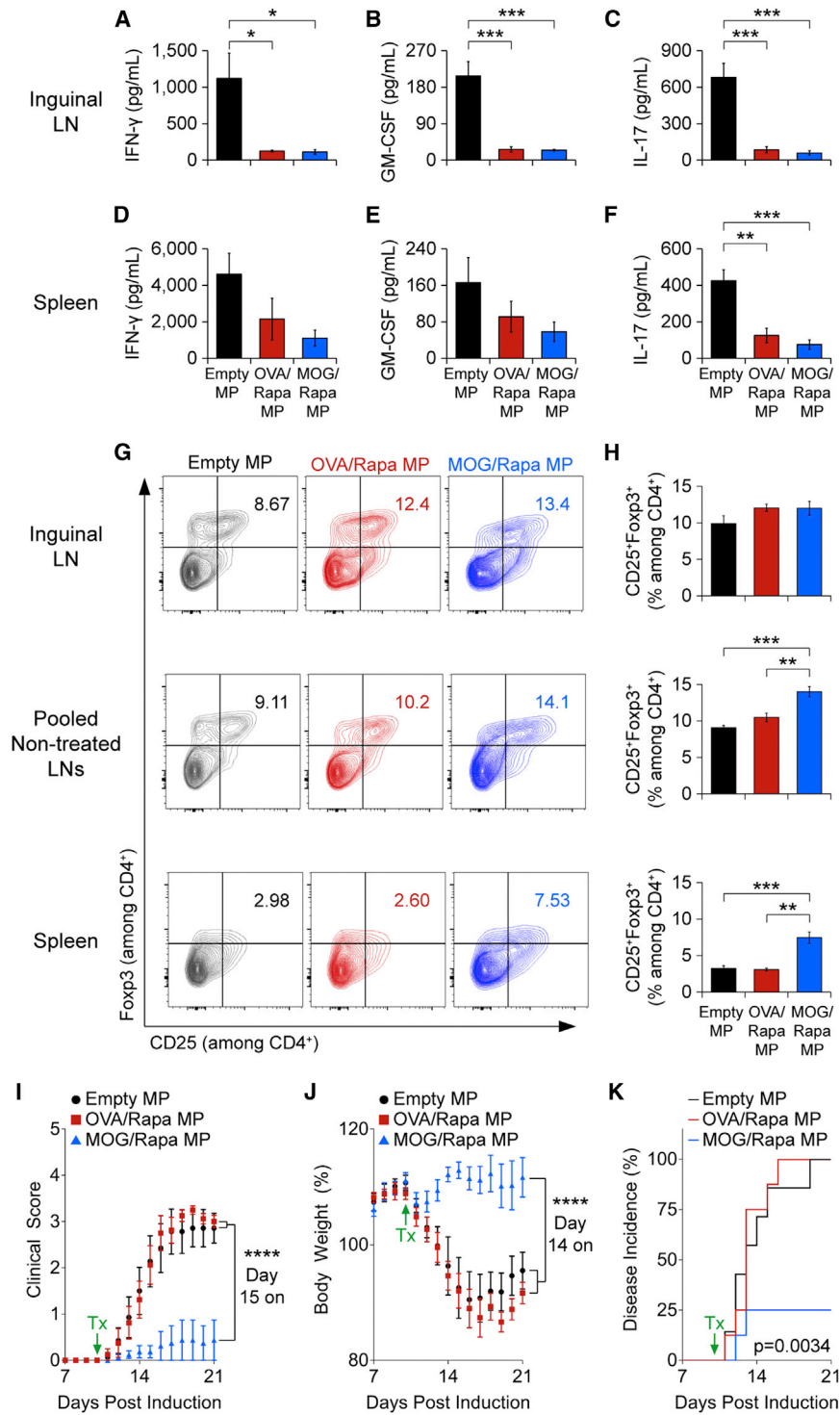
**Figure 5. Incorporation of Self-Antigen Is Required for T_REG Induction and Attenuation of Disease, but Not for Local Suppression of Inflammation**

(A–C) Mice were induced with EAE and treated *i.LN.* on day 10 with empty MPs, OVA/Rapa MPs, or MOG/Rapa MPs (n = 4 for each MP formulation). On day 21, cells were isolated from treated LNs and restimulated with MOG peptide, and secretion of (A) IFN-$\gamma$, (B) GM-CSF, and (C) IL-17 was measured.

(D–F) Similar analyses were performed on cells isolated from splenocytes.

(G and H) The (G) scatterplots and (H) mean T_REG (CD25$^+$Foxp3$^+$ among CD4$^+$) frequencies in treated inguinal LNs (top), non-treated axillary and brachial LNs (middle), and spleens (bottom) after *i.LN.* injection on day 10 post-EAE induction and analysis on day 12, are shown (n = 4–6 for each MP formulation).

(I–K) The (I) mean clinical score, (J) relative body weight, and (K) disease incidence of mice induced with EAE and treated *i.LN.* on day 10 (Tx, green arrows) with empty MPs (n = 7), OVA/Rapa MPs (n = 8), or MOG/Rapa MPs (n = 8). Statistical analyses in (A)–(F) and (H) were performed using one-way ANOVA with a Tukey post-test; all statistically significant differences are indicated. Statistical analyses in (I) and (J) were performed using two-way ANOVA with a Tukey post-test and in (K) using a log-rank test. Data in all panels represent mean ± SEM (*p $\leq$ 0.05, **p $\leq$ 0.01, ***p $\leq$ 0.001, and ****p $\leq$ 0.0001).

See also Figure S5.

example, peripheral blood mononuclear cells coupled to myelin peptides, or patient-specific, myelin-reactive, irradiated T cells. In parallel, several preclinical reports describe soluble treatments or biomaterial-based approaches to deliver self-antigen, regulatory small molecules, or both to restrain self-reactivity (Clemente-Casares et al., 2016; Esposito et al., 2010; Gammon et al., 2015; Getts et al., 2012, 2014; Ho et al., 2005; Hunter et al., 2014; Maldonado et al., 2015; Tsai et al., 2010; Yeste et al., 2012). While these approaches demonstrate exciting opportunities for translation toward the goal of more effective and selective control of human disease, the approaches reflect different strategies in the immuno-modulatory signals delivered. As noted, some studies demonstrate co-delivery of self-antigen and a regulatory signal confers therapeutic effects (Maldonado et al., 2015; Yeste et al., 2012), while other reports suggest that changing the physical form of self-antigen can trigger existing debris clearance pathways to promote tolerance in the absence of explicit immunoregulatory cues (Getts et al., 2012, 2014; Hunter et al., 2014). Further, studies in animal

## DISCUSSION

The need for more effective and selective treatments for MS has stimulated new clinical trials aimed at myelin-specific or personalized therapies (Lutterotti and Martin, 2014). These approaches focus on cell-based adoptive transfer strategies, for
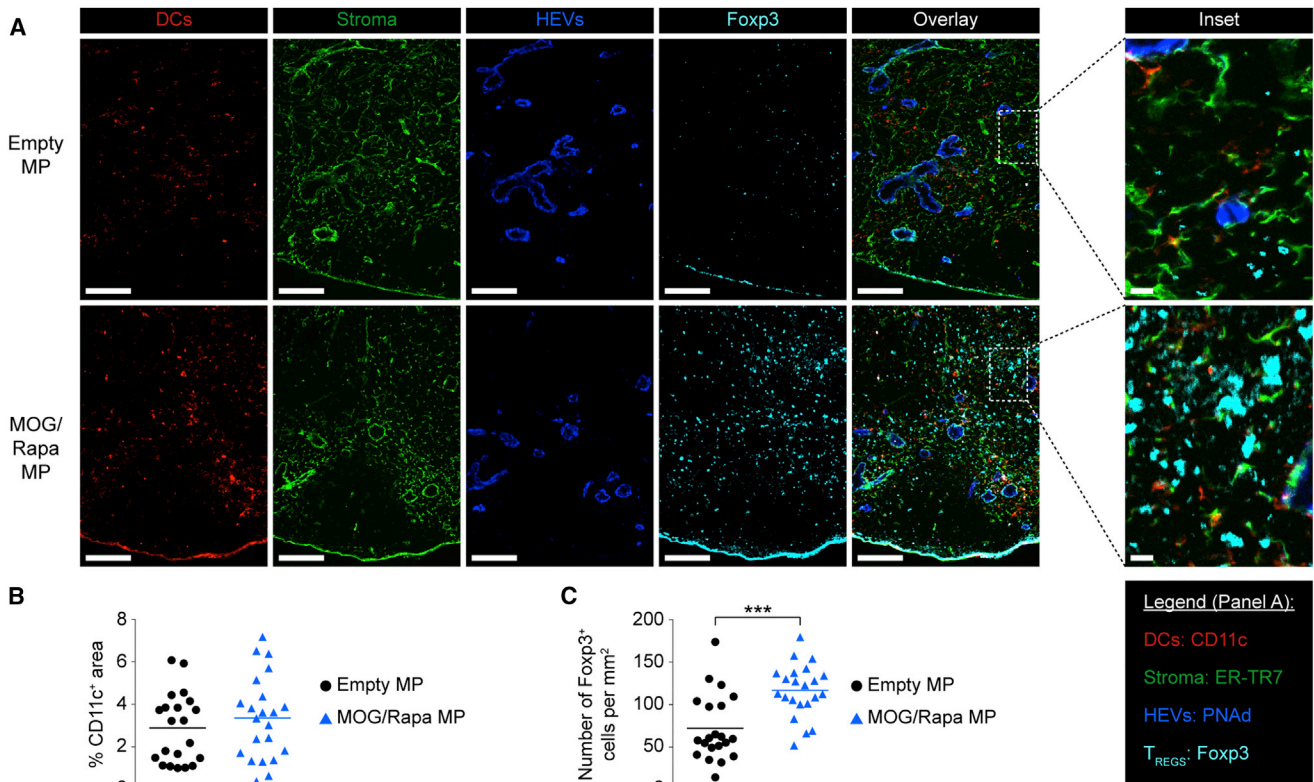
**Figure 6. MOG/Rapa MPs Promote Tolerogenic Reorganization and Accumulation of T_REGS in CNS-Draining LNs**

Mice were induced with EAE and treated *i.LN.* on day 10 with empty MPs or MOG/Rapa MPs (n = 4), and cervical LNs were excised for analysis 5 days later.
(A) Immunofluorescent analysis of cervical LNs shows DCs (CD11c⁺, red), reticular fibroblasts (stroma, ER-TR7⁺, green), HEVs (PNAd⁺, blue), Foxp3⁺ cells (cyan), and an overlay. Scale bars, 100 µm. An inset of the overlay channel is shown on the far right column. Scale bar, 10 µm.
(B and C) Quantitative image analysis was used determine the frequency of (B) DCs and (C) Foxp3 following empty MP (n = 21) or MOG/Rapa MP (n = 22) treatment in the cortical ridge of sections like the representative images shown in (A). Statistical analyses were two-tailed Student's t tests.

models and human MS identify the presence of myelin self-antigen in LNs (Korn et al., 2007; Mohammad et al., 2014; van Zwam et al., 2009b). These results indicate that CNS antigens are present in peripheral sites of T cell polarization during disease, suggesting that delivery of tolerogenic signals alone may be sufficient to restrain myelin-specific self-attack. Thus, the role of candidate immunomodulatory signals and combinations of these signals is not well defined, particularly in the context of the impact on the LN microenvironment.

The connections between systemic tolerance and local LN function are of particular interest to MS, since pathogenic T cells are armed in LNs prior to CNS infiltration. Past studies, for example, revealed that excision of CNS-draining LNs restricts T cell infiltration to the CNS and limits EAE in rat models (van Zwam et al., 2009a). In addition, recent work has identified APCs and T cells in newly discovered lymphatics that connect the CNS with cervical LNs outside the CNS (Aspelund et al., 2015; Louveau et al., 2015). These findings, along with human trials using *i.LN.* injection of free antigens for cancer or allergy therapy (Senti and Kündig, 2015), suggest clinical opportunities based on controlling the local response to myelin in LNs during MS as a direct route to promote myelin-specific tolerance. Thus, one outcome of our work is a new possibility for locally pro-

gramming LN function, through co-delivery from depots, local controlled release, or other biomaterial-enabled features, to generate systemic and specific control of disease. In addition to assessing clinical potential, we sought to use *i.LN.* depots as a tool to study how the local inflammatory or tolerogenic state of LNs controls the magnitude and specificity of systemic tolerance. This platform provides a unique opportunity to probe the spatial and temporal dynamics of immune response to self-antigens; in contrast, approaches that employ systemic injections or repeated doses complicate these kinds of perturbations.

Our experiments reveal that reprogramming discrete LNs can generate systemic tolerance. The dependence of therapeutic efficacy on *i.LN.* delivery of encapsulated, disease-relevant self-antigen highlights three unique results of this platform. First, a role for controlled kinetic release from micron-scale depots retained in LNs following injection (Andorko et al., 2014; Jewell et al., 2011) is supported by the observation that substitution of soluble myelin self-antigen eliminates therapeutic efficacy (Figure 4). Second, perhaps in parallel, direct deposition of MPs in LNs may drive higher frequency encounters with resident APC populations that have been shown to promote tolerance (Maldonado et al., 2015). This approach might provide a means to bypass the relatively inefficient drainage and trafficking
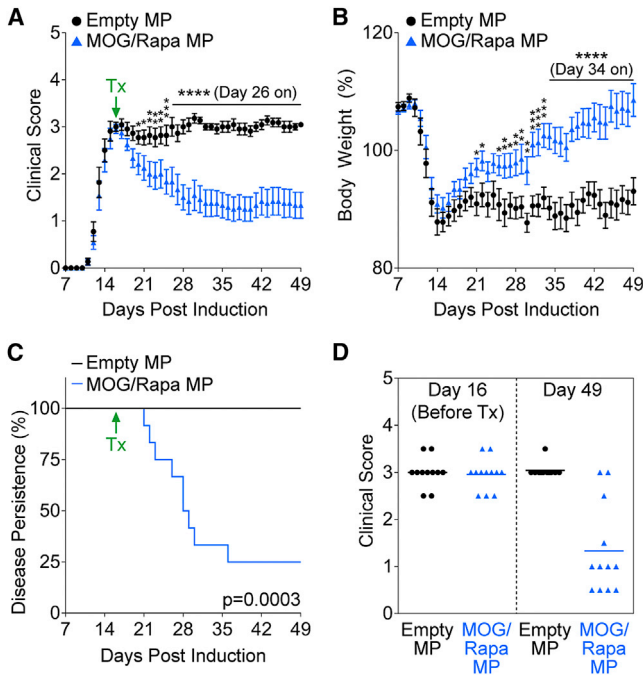
**Figure 7. A Single *i.LN.* Dose of MOG/Rapa MPs Reverses Disease-Induced Paralysis**

(A and B) Mice were treated at the peak of EAE (day 16; Tx, green arrow) using a single *i.LN.* dose of empty MPs (n = 11) or MOG/Rapa MPs (n = 12), and (A) mean clinical score and (B) weight were monitored.

(C) Persistence of disease is shown, with recovery from disease defined as at least a two-point reduction in clinical score relative to the score just prior to treatment.

(D) Score distribution of mice in (A)–(C) just before treatment (day 16, left) and at day 49 (right).

Statistical analysis in (A) and (B) was performed using multiple t tests, one at each time point, with a Holm-Sidak post-test correction for multiple comparisons, and in (C) using a log-rank test. Data in all panels represent mean ± SEM (*p $\leq$ 0.05, **p $\leq$ 0.01, ***p $\leq$ 0.001, and ****p $\leq$ 0.0001).

mechanisms by which signals traditionally reach LNs and spleen following peripheral injection (Andorko et al., 2014, 2015; Jewell et al., 2011) and, therefore, enhance efficacy compared with i.m. delivery of a matched dose tested here (Figure 4). Third, the observation that both MOG MPs and MOG/Rapa co-loaded MPs attenuate disease (Figure 1) suggests a possible contribution from altered trafficking or more efficient processing of antigen in particulate form relative to soluble antigen (Getts et al., 2012, 2014; Hunter et al., 2014).

In addition to the need for encapsulation and targeted LN injection, ex vivo restimulation further revealed a less inflammatory milieu was established in LNs by MOG/Rapa depots (Figures 4A–4C and 5A–5C). We observed a decrease in the myelin-triggered secretion of three key cytokine drivers of inflammation during disease in mice and humans (IL-17, IFN-$\gamma$, and GM-CSF). In particular, IL-17 is a characteristic cytokine secreted by $T_H17$ cells, while IFN-$\gamma$ is a broad pro-inflammatory signal secreted by $T_H1$ subsets during autoimmunity (Dendrou et al., 2015). Further, GM-CSF has been shown to be secreted by self-reactive T helper cells, triggering an inflammatory

cascade that enhances pathogenic monocyte-derived cell infiltration into the CNS and subsequent tissue damage (Croxford et al., 2015). Together, these findings support a possible mechanism by which myelin is presented in LNs but whereby the response is altered by the presence of $T_{REG}$-inducing signals in the case of MOG/Rapa MPs, or at least a lack of co-stimulation in the case of MOG MPs. Supporting this idea, we discovered that MOG/Rapa MPs drive distinct remodeling of the LN stroma, with Foxp3+ cells accumulating in the cortical ridge of LNs in close proximity to high endothelial venules (HEVs)—routes of T cell entry into LNs (Warren et al., 2014). Our measurements of this phenomenon in treated LNs (Figures 4D and 4F) and non-treated, CNS-draining LNs (Figures 6A and 6C) suggest that local perturbation of LNs with self-antigen and Rapa promotes this tolerogenic reorganization.

After *i.LN.* injection of MOG/Rapa MPs, we also observed a significant increase in the frequency of $T_{REGS}$ in the spleen and pooled non-treated LNs relative to empty MPs or OVA/Rapa MPs (Figures 5G and 5H). This result further underscores the self-antigen-specific nature of efficacy, though new tools such as MHC-II tetramer could help directly verify the antigen specificity of T cell receptors (TCRs) on the expanding $T_{REGS}$ (Nelson et al., 2015). Interestingly, effects were least pronounced and statistically insignificant in treated LNs (Figures 5G and 5H, top). One explanation for this outcome may be that local delivery of myelin triggers resident myelin-reactive cells but little expansion of regulatory cells occurs because Rapa inhibits proliferation. This hypothesis is supported by the discovery that, while MPs encapsulating Rapa and the irrelevant antigen OVA did not impact disease (Figures 5I and 5K), these particles caused local suppression of inflammatory recall response equivalent to that of MOG/Rapa MPs (Figures 5A–5C) in treated nodes. There was an intermediate reduction in the spleen, an untreated site, likely due to non-specific, systemic effects of Rapa. Supporting this hypothesis, recent literature demonstrates that systemic treatments with modulatory or suppressive drugs can cause differential impacts on inflammatory responses in different tissues, findings that also illustrate the utility of having a tool to directly probe how signals in one tissue impact the course, efficiency, and durability of tolerance (White et al., 2014). One further rationale for co-delivery of tolerogenic signals (e.g., Rapa) with self-antigen is to mitigate the risk of exacerbating disease with a therapy containing disease-relevant antigen during active autoimmunity (Maldonado et al., 2015).

Our findings reveal antigen-specific tolerance can be generated with striking efficacy by locally reprogramming LNs, results demonstrating the unique potential of this strategy to study and combat autoimmunity. Some of the important follow-up studies include the need to further assess the trafficking of T cells from treated LNs to the cervical LNs and CNS, and importantly, to confirm remyelination, a critical criterion for human MS therapy. The functional selectivity of tolerance also should be assessed by confirming intact pro-immune responses to exogenous antigens after recovery. Lastly, mouse models do not fully recapitulate the myelin reactivity and epitope spreading present in human disease. The modular nature of the engineering approach reported here allows facile incorporation of multiple peptide epitopes and could support future studies in other models or in humans to

assess these dynamics. Thus, this work demonstrates unique potential to study, control, and reverse established autoimmune disease in a selective fashion by modulating local LN function.

## EXPERIMENTAL PROCEDURES

### Materials and Reagents

Myelin oligodendrocyte glycoprotein ($MOG_{35-55}$) and ovalbumin ($OVA_{323-339}$) peptides, with or without a fluorescein isothiocyanate (FITC) tag conjugated to the N terminus, were synthesized by GenScript at $\geq$98% purity. Poly(lactide-co-galactide) (PLGA) and poly(vinyl alcohol) (PVA) were purchased from Sigma. Rapa was purchased from LC Laboratories. Antibodies for flow cytometry, including CD16/CD32, V450 CD4 (clone RM4-5), PE-Cy7 CD25 (clone PC61), Alexa Fluor 488 Foxp3 (clone MF23), PE-Cy7 CD3 (clone 145-2C11), FITC CD4 (clone RM4-5), PE CD8 (clone 53-6.7), PE F4/80 (clone T45-2342), and allophycocyanin-Cy7 CD11c (clone HL3), were purchased from BD Biosciences.

### Particle Synthesis

Double-emulsion/solvent evaporation was used to generate degradable PLGA MPs as previously reported (Andorko et al., 2014; Jewell et al., 2011). Briefly, an inner aqueous phase was prepared as either 500 $\mu$l water or 1 mg peptide (i.e., MOG or OVA) dissolved in 500 $\mu$l water. The inner aqueous phase was sonicated with an organic phase comprised of 80 mg PLGA dissolved in 5 ml dichloromethane for 30 s at 12 W to form a water/oil emulsion. In MP formulations containing Rapa, polymer solution was added to a vial containing 2 mg dried drug before sonication to incorporate Rapa into the organic phase. For all formulations, the primary emulsion was homogenized with 40 ml 2% PVA for 3 min at 16,000 rpm to form final, stabilized double emulsions. Particles were stirred for 16 hr to allow for solvent evaporation. After 16 hr, MPs were poured through a 40-$\mu$m cell strainer to remove any aggregates and collected by centrifugation (5 min, 5,000 $\times$ $g$, and 4°C). The supernatants were decanted and MPs were washed three times with 1 ml water, collected by centrifugation between each wash, and resuspended in water.

### Particle Characterization

Particle size was measured using an LA-950 laser diffraction size analyzer (Horiba). A known aliquot of MPs was dried under air, and the dry mass was used to calculate the total particle yield and normalized to the polymer input (i.e., percentage yield). The loading of peptide was quantified via Micro BCA Protein Assay Kit (Thermo Scientific Pierce) as previously described (Sah, 1997). The loading of Rapa was measured via UV/Vis spectrophotometry after dissolution of a known mass of dried particles in DMSO. For all cargos, standard curves of known concentrations were used to calculate loading, reported as the mass of cargo per mass of particles and normalized to the input to synthesis (i.e., encapsulation efficiency). For studies involving immunofluorescent analysis of intra-nodal MP deposition, fluorescently tagged MOG peptide (FITC-MOG) was incorporated into the inner aqueous phase, and 10 $\mu$l fluorescent dye (Vybrant DiI Cell-Labeling Solution, Molecular Probes) was added to the organic phase of MP synthesis to enable visualization of particles and encapsulated cargo in tissue sections.

### EAE Induction and Monitoring

EAE was induced in 10- to 11-week-old female C57BL/6J mice (The Jackson Laboratory) according to the manufacturer's instructions (Hooke Laboratories). Briefly, on day 0, mice were administered two subcutaneous injections of an emulsion of complete Freund's adjuvant and a peptide fragment of MOG ($MOG_{35-55}$). Then 2 and 24 hr later, mice were administered pertussis toxin via intraperitoneal injections. Beginning 7 days after induction, mice were monitored daily for weight fluctuation and symptoms of paralysis, which were assigned a clinical score to reflect disease severity (0, no symptoms; 1, limp tail; 2, hind limb weakness; 3, hind limb paralysis; 4, full hind limb and partial front limb paralysis; and 5, moribund). Incidence of disease was defined as the first day a mouse exhibited a clinical score >0, and it was reported as the percentage of mice in each group with detectable symptoms of disease over time. Mean

maximum score of each group was calculated by averaging the maximum score reached throughout the duration of the experiment of each mouse.

### Immunizations

Doses of MP formulations were administered via non-surgical, direct *i.LN.* injection as we previously described (Andorko et al., 2014; Jewell et al., 2011). Briefly, 1 day prior to injection, mice were administered a bilateral injection of tracer dye (Evans blue, Alfa Aesar) subcutaneously at the tail base and their fur was removed with a mild depilatory cream. On the day of treatment, each mouse received a single dose of indicated MP formulations, dissolved in the appropriate final injection volume (2 $\times$ 10 $\mu$l). Immunizations were administered as bilateral injections to the inguinal LNs, with each LN receiving half of the total dose. Irrespective of formulation, each mouse was treated with 2 mg MPs (i.e., 1 mg per LN), containing the indicated cargos at the levels shown in Table S1. In control studies, matched masses of MPs were administered via bilateral i.m. injections in the caudal thigh, with injection volumes adjusted to 2 $\times$ 25 $\mu$l.

### Tissue Processing

At the indicated time points, injected inguinal LNs, spleen, and, in some cases, non-treated axillary and brachial LNs were excised and processed by manual dissociation through a 40-$\mu$m cell strainer. Cells were collected by centrifugation (5 min, 800 $\times$ $g$, and 4°C). Spleen samples were resuspended in Ack lysing buffer (Invitrogen) to remove red blood cells and then washed with PBS. LN cells were washed with PBS without lysis. Cells were counted using an automated cell counter (NanoEnTek) or counting beads according to the manufacturer's instructions (BD Biosciences), and they were either plated for ex vivo restimulation assays or analyzed immediately by flow cytometry.

### Ex Vivo Restimulation Assays

To characterize cellular response after an encounter of disease-relevant (i.e., MOG) or irrelevant (i.e., OVA) antigen, a uniform number of cells ($1 \times 10^6$) was plated from each tissue sample in duplicate. One well was restimulated in culture with MOG (25 $\mu$g/ml) and the second well received a matched dose of OVA peptide. After 48 hr of incubation, culture supernatants were collected for analysis by ELISA.

### ELISA

All ELISAs were performed according to the manufacturer's instructions for IL-17 (R&D Systems), GM-CSF (R&D Systems), and IFN-$\gamma$ (BD Biosciences) detection. Supernatants were collected from cell culture samples and analyzed at 1–20$\times$ dilutions.

### Flow Cytometry Experiments

Immediately after tissue excision and processing, cells were washed with 200 $\mu$l 1% BSA in 1×PBS, resuspended in Fc block (anti-CD16/CD32), and incubated for 10 min at room temperature to inhibit non-specific binding. Cells were then incubated with the indicated antibodies against cell surface markers, including CD3, CD4, CD8, F4/80, CD11c, and CD25. Cells were washed to remove unbound antibody, and then stained for viability (DAPI, Invitrogen) and analyzed immediately or fixed and permeabilized to enable staining for intracellular markers (i.e., transcription factors). After fixation and permeabilization (Foxp3/Transcription Factor Staining Buffer Set, eBioscience), cells were stained for expression of Foxp3, washed, and analyzed. All analysis was performed on a FACS Canto II (BD Biosciences) and data analysis was conducted using FlowJo version 10 (Tree Star).

### Immunofluorescent Analysis

At the indicated time points, treated inguinal LNs, non-treated cervical LNs, or spinal cords were excised and immediately submerged in OCT compound (Tissue-Tek) and frozen. Cryosections were cut at 6 $\mu$m using a Microm HM 550 cryostat (Thermo Fisher Scientific). Sections were fixed with cold acetone for 5 min, washed with PBS, and blocked with 5% donkey serum (Sigma) and 5% goat serum (Sigma) in PBS for 30 min. Following a PBS wash, samples were stained for 1 hr with primary antibodies against the indicated markers, including T cells (CD3e, Rb pAb, Abcam), B cells (B220, clone RA3-6B2, eBioscience), DCs (CD11c, Ham pAb, BD Pharmingen), HEVs

(PNAd, clone MECA-79, BD Pharmingen), stroma (ER-TR7, clone sc-73355, Santa Cruz Biotechnology), and Foxp3 (Rb pAb, Abcam). Sections were washed once with PBS and fluorescently conjugated secondary Ab was applied for 45 min. Slides were washed three times in PBS for 5 min, fixed with 4% paraformaldehyde (Electron Microscopy Sciences), treated with 1% glycerol in PBS before mounting with Prolong Diamond Antifade Mountant (LifeSciences), in some cases containing DAPI, and imaged using a confocal microscope.

For quantitative analyses, tissues were collected 5 days after *i.LN.* injection (i.e., day 15) of either empty MPs or MOG/Rapa MPs (n = 4 mice; eight injected inguinal LNs, at least 16 cervical LNs, and four spinal cords). Quantitative analysis was performed on images of treated inguinal LNs, cervical LNs, and spinal cords using Volocity image analysis software (PerkinElmer). For LN analyses, the percentage of $CD11c^+$ area was defined as the fraction of tissue area staining positive for CD11c among cortical ridge area, defined as the area positive for ER-TR7. The threshold for positive area for both signals was defined using appropriate iso-type control-stained sections. The number of $Foxp3^+$ cells among the cortical ridge was similarly quantified using an iso-type control to define positive cells. In spinal cord analyses, the percentage of $CD3^+$ area was defined as the fraction of area staining positive for CD3 among the total spinal cord area imaged. Similarly, an iso-type control was used to set the threshold for positive area. All quantitative analysis was performed on at least 20 images of LN or spinal cord per MP formulation, and statistical analyses were performed using two-tailed Student's t tests.

### In Vivo Study Design

On the day of induction, mice were screened to identify animals with the most consistent starting body weights to be included in the study. Mice were then induced with EAE, as described above, and randomized into treatment groups. In studies involving late-stage therapy, the clinical scores of mice were assessed and mice were randomized into two groups with equivalent mean scores just before treatment. Mice were removed from studies according to humane endpoints, including loss of $\geq 25\%$ of initial (day 0) body weight, presentation with a clinical score of 4 for 2 consecutive days, or presentation with a clinical score of 4.5 or 5 on a single day. In mechanistic studies designed to investigate the kinetics of disease or tolerance, mice were induced with EAE, randomized into groups, and identically treated groups of mice were euthanized at the indicated time points for analysis. Data collection and analyses were not blinded and no outliers were excluded.

### Statistics

Student's t tests were used in comparisons of two groups and ANOVA was used to compare three or more groups, with post-test corrections for multiple comparisons as indicated in figure captions. Log-rank tests were used in analyses of disease incidence or persistence. All tests were two-sided analyses and were performed using GraphPad Prism software. Error bars in all panels represent mean ± SEM and p values $\leq 0.05$ were considered significant.

### Study Approval

All animal studies were carried out under the supervision of the University of Maryland Institutional Animal Care and Use Committee (IACUC) in compliance with local, state, and federal guidelines.

### SUPPLEMENTAL INFORMATION

Supplemental Information includes five figures and one table and can be found with this article online at http://dx.doi.org/10.1016/j.celrep.2016.08.033.

### AUTHOR CONTRIBUTIONS

L.H.T. performed all experiments and statistical analysis. Y.-C.C. and J.M.G. contributed to animal experiments. T.S. and J.I.A. performed immunofluorescent analysis of LNs. L.H.T. and C.M.J. designed the experiments and wrote the manuscript. All authors contributed to data analysis and manuscript preparation.

### REFERENCES

Andorko, J.I., Tostanoski, L.H., Solano, E., Mukhamedova, M., and Jewell, C.M. (2014). Intra-lymph node injection of biodegradable polymer particles. J. Vis. Exp. *83*, e50984.

Andorko, J.I., Hess, K.L., and Jewell, C.M. (2015). Harnessing biomaterials to engineer the lymph node microenvironment for immunity or tolerance. AAPS J. *17*, 323–338.

Aspelund, A., Antila, S., Proulx, S.T., Karlsen, T.V., Karaman, S., Detmar, M., Wiig, H., and Alitalo, K. (2015). A dural lymphatic vascular system that drains brain interstitial fluid and macromolecules. J. Exp. Med. *212*, 991–999.

Clemente-Casares, X., Blanco, J., Ambalavanan, P., Yamanouchi, J., Singha, S., Fandos, C., Tsai, S., Wang, J., Garabatos, N., Izquierdo, C., et al. (2016). Expanding antigen-specific regulatory networks to treat autoimmunity. Nature *530*, 434–440.

Comabella, M., and Khoury, S.J. (2012). Immunopathogenesis of multiple sclerosis. Clin. Immunol. *142*, 2–8.

Cross, A.H., and Naismith, R.T. (2014). Established and novel disease-modifying treatments in multiple sclerosis. J. Intern. Med. *275*, 350–363.

Croxford, A.L., Lanzinger, M., Hartmann, F.J., Schreiner, B., Mair, F., Pelczar, P., Clausen, B.E., Jung, S., Greter, M., and Becher, B. (2015). The cytokine GM-CSF drives the inflammatory signature of CCR2+ monocytes and licenses autoimmunity. Immunity *43*, 502–514.

Dendrou, C.A., Fugger, L., and Friese, M.A. (2015). Immunopathology of multiple sclerosis. Nat. Rev. Immunol. *15*, 545–558.

Esposito, M., Ruffini, F., Bellone, M., Gagliani, N., Battaglia, M., Martino, G., and Furlan, R. (2010). Rapamycin inhibits relapsing experimental autoimmune encephalomyelitis by both effector and regulatory T cells modulation. J. Neuroimmunol. *220*, 52–63.

Gammon, J.M., Tostanoski, L.H., Adapa, A.R., Chiu, Y.C., and Jewell, C.M. (2015). Controlled delivery of a metabolic modulator promotes regulatory T cells and restrains autoimmunity. J. Control. Release *210*, 169–178.

Getts, D.R., Martin, A.J., McCarthy, D.P., Terry, R.L., Hunter, Z.N., Yap, W.T., Getts, M.T., Pleiss, M., Luo, X., King, N.J., et al. (2012). Microparticles bearing encephalitogenic peptides induce T-cell tolerance and ameliorate experimental autoimmune encephalomyelitis. Nat. Biotechnol. *30*, 1217–1224.

Getts, D.R., Terry, R.L., Getts, M.T., Deffrasnes, C., Müller, M., van Vreden, C., Ashhurst, T.M., Chami, B., McCarthy, D., Wu, H., et al. (2014). Therapeutic inflammatory monocyte modulation using immune-modifying microparticles. Sci. Transl. Med. *6*, 219ra7.

Ho, P.P., Fontoura, P., Platten, M., Sobel, R.A., DeVoss, J.J., Lee, L.Y., Kidd, B.A., Tomooka, B.H., Capers, J., Agrawal, A., et al. (2005). A suppressive oligodeoxynucleotide enhances the efficacy of myelin cocktail/IL-4-tolerizing DNA vaccination and treats autoimmune disease. J. Immunol. *175*, 6226–6234.

Hunter, Z., McCarthy, D.P., Yap, W.T., Harp, C.T., Getts, D.R., Shea, L.D., and Miller, S.D. (2014). A biodegradable nanoparticle platform for the induction of antigen-specific immune tolerance for treatment of autoimmune disease. ACS Nano *8*, 2148–2160.

Jewell, C.M., López, S.C., and Irvine, D.J. (2011). In situ engineering of the lymph node microenvironment via intranodal injection of adjuvant-releasing polymer particles. Proc. Natl. Acad. Sci. USA *108*, 15745–15750.

Kontos, S., Kourtis, I.C., Dane, K.Y., and Hubbell, J.A. (2013). Engineering antigens for in situ erythrocyte binding induces T-cell deletion. Proc. Natl. Acad. Sci. USA *110*, E60–E68.

Korn, T., Reddy, J., Gao, W., Bettelli, E., Awasthi, A., Petersen, T.R., Bäckström, B.T., Sobel, R.A., Wucherpfennig, K.W., Strom, T.B., et al. (2007). Myelin-specific regulatory T cells accumulate in the CNS but fail to control autoimmune inflammation. Nat. Med. *13*, 423–431.

Look, M., Stern, E., Wang, Q.A., DiPlacido, L.D., Kashgarian, M., Craft, J., and Fahmy, T.M. (2013). Nanogel-based delivery of mycophenolic acid ameliorates systemic lupus erythematosus in mice. J. Clin. Invest. *123*, 1741–1749.

Louveau, A., Smirnov, I., Keyes, T.J., Eccles, J.D., Rouhani, S.J., Peske, J.D., Derecki, N.C., Castle, D., Mandell, J.W., Lee, K.S., et al. (2015). Structural and functional features of central nervous system lymphatic vessels. Nature *523*, 337–341.

Lutterotti, A., and Martin, R. (2014). Antigen-specific tolerization approaches in multiple sclerosis. Expert Opin. Investig. Drugs *23*, 9–20.

Maldonado, R.A., LaMothe, R.A., Ferrari, J.D., Zhang, A.H., Rossi, R.J., Kolte, P.N., Griset, A.P., O'Neil, C., Altreuter, D.H., Browning, E., et al. (2015). Polymeric synthetic nanoparticles for the induction of antigen-specific immunological tolerance. Proc. Natl. Acad. Sci. USA *112*, E156–E165.

Manicassamy, S., and Pulendran, B. (2011). Dendritic cell control of tolerogenic responses. Immunol. Rev. *241*, 206–227.

Mohammad, M.G., Tsai, V.W., Ruitenberg, M.J., Hassanpour, M., Li, H., Hart, P.H., Breit, S.N., Sawchenko, P.E., and Brown, D.A. (2014). Immune cell trafficking from the brain maintains CNS immune tolerance. J. Clin. Invest. *124*, 1228–1241.

Mueller, S.N., and Germain, R.N. (2009). Stromal cell contributions to the homeostasis and functionality of the immune system. Nat. Rev. Immunol. *9*, 618–629.

Nelson, R.W., Beisang, D., Tubo, N.J., Dileepan, T., Wiesner, D.L., Nielsen, K., Wüthrich, M., Klein, B.S., Kotov, D.I., Spanier, J.A., et al. (2015). T cell receptor cross-reactivity between similar foreign and self peptides influences naive cell population size and autoimmunity. Immunity *42*, 95–107.

Northrup, L., Sestak, J.O., Sullivan, B.P., Thati, S., Hartwell, B.L., Siahaan, T.J., Vines, C.M., and Berkland, C. (2014). Co-delivery of autoantigen and b7 pathway modulators suppresses experimental autoimmune encephalomyelitis. AAPS J. *16*, 1204–1213.

Northrup, L., Christopher, M.A., Sullivan, B.P., and Berkland, C. (2016). Combining antigen and immunomodulators: Emerging trends in antigen-specific immunotherapy for autoimmunity. Adv. Drug Deliv. Rev. *98*, 86–98.

Piehl, F. (2014). A changing treatment landscape for multiple sclerosis: challenges and opportunities. J. Intern. Med. *275*, 364–381.

Sah, H. (1997). A new strategy to determine the actual protein content of poly(lactide-co-glycolide) microspheres. J. Pharm. Sci. *86*, 1315–1318.

Senti, G., and Kündig, T.M. (2015). Intralymphatic immunotherapy. World Allergy Organ. J. *8*, 9.

Steinman, L., Merrill, J.T., McInnes, I.B., and Peakman, M. (2012). Optimization of current and future therapy for autoimmune diseases. Nat. Med. *18*, 59–65.

Tsai, S., Shameli, A., Yamanouchi, J., Clemente-Casares, X., Wang, J., Serra, P., Yang, Y., Medarova, Z., Moore, A., and Santamaria, P. (2010). Reversal of autoimmunity by boosting memory-like autoregulatory T cells. Immunity *32*, 568–580.

van Zwam, M., Huizinga, R., Heijmans, N., van Meurs, M., Wierenga-Wolf, A.F., Melief, M.J., Hintzen, R.Q., 't Hart, B.A., Amor, S., Boven, L.A., and Laman, J.D. (2009a). Surgical excision of CNS-draining lymph nodes reduces relapse severity in chronic-relapsing experimental autoimmune encephalomyelitis. J. Pathol. *217*, 543–551.

van Zwam, M., Huizinga, R., Melief, M.J., Wierenga-Wolf, A.F., van Meurs, M., Voerman, J.S., Biber, K.P., Boddeke, H.W., Höpken, U.E., Meisel, C., et al. (2009b). Brain antigens in functionally distinct antigen-presenting cell populations in cervical lymph nodes in MS and EAE. J. Mol. Med. *87*, 273–286.

Warren, K.J., Iwami, D., Harris, D.G., Bromberg, J.S., and Burrell, B.E. (2014). Laminins affect T cell trafficking and allograft fate. J. Clin. Invest. *124*, 2204–2218.

White, M., Webster, G., O'Sullivan, D., Stone, S., and La Flamme, A.C. (2014). Targeting innate receptors with MIS416 reshapes Th responses and suppresses CNS disease in a mouse model of multiple sclerosis. PLoS ONE *9*, e87712.

Yeste, A., Nadeau, M., Burns, E.J., Weiner, H.L., and Quintana, F.J. (2012). Nanoparticle-mediated codelivery of myelin antigen and a tolerogenic small molecule suppresses experimental autoimmune encephalomyelitis. Proc. Natl. Acad. Sci. USA *109*, 11270–11275.